ENVIRONMENTAL RESEARCH
LETTERS

PURPOSE-LED PUBLISHING™

LETTER · OPEN ACCESS

Precipitation leads the long-term vegetation increase in the conterminous United States drylands

To cite this article: Yuhe Chang *et al* 2025 *Environ. Res. Lett.* **20** 044006

View the article online for updates and enhancements.

You may also like

- Overestimated global dryland expansion with substantial increases in vegetation productivity under climate warming
Ziwei Liu, Taihua Wang and Hanbo Yang
- Distinct vegetation response to drying and wetting trends across an aridity threshold
Wei Zhao, Xiubo Yu, Yu Liu et al.
- The PMIP4 simulated dryland aridity changes during the Last Interglacial
Shanshan Liu and Xuecheng Zhou

This content was downloaded from IP address 108.26.195.223 on 12/04/2025 at 13:31

IOP Publishing Environ. Res. Lett. 20 (2025) 044006 https://doi.org/10.1088/1748-9326/adb985

ENVIRONMENTAL RESEARCH
LETTERS

LETTER

Precipitation leads the long-term vegetation increase in the conterminous United States drylands

Yuhe Chang[1,*], **Alexander J Winkler**[2], **Amirhossein Noori**[1], **Yuri Knyazikhin**[1] and **Ranga B Myneni**[1]

[1] Department of Earth and Environment, Boston University, Boston, MA 02155, United States of America
[2] Max-Planck-Institute for Biogeochemistry, 07745 Jena, Germany
[*] Author to whom any correspondence should be addressed.

E-mail: yhchang@bu.edu

Keywords: precipitation, drylands, rain use efficiency, CO_2 fertilization effect, greening

Supplementary material for this article is available online

OPEN ACCESS

RECEIVED
25 October 2024

REVISED
3 February 2025

ACCEPTED FOR PUBLICATION
24 February 2025

PUBLISHED
11 March 2025

Original content from this work may be used under the terms of the Creative Commons Attribution 4.0 licence.

Any further distribution of this work must maintain attribution to the author(s) and the title of the work, journal citation and DOI.

Abstract

Drylands, encompassing over 40% of the conterminous United States (CONUS), are crucial to the global carbon cycle and highly susceptible to climate change. However, Earth system models offer conflicting projections of future drought and vegetation activity in North America, and in-depth analyses of the long-term changes in greenness and its relationship with underlying climate drivers, considering both spatial and temporal variations at the ecosystem scale, are lacking. This study analyzes 20 year (2001–2020) MODIS normalized difference vegetation index (NDVI) observations to assess greenness trends in CONUS drylands and their relationship with climate drivers at 1 km spatial resolution. Results indicate a large scale and systematic greening trend, particularly in the northern Great Plains (NGP) region. Using an empirical linear attribution approach and empirical orthogonal function analysis, we uncover varied relationships between greenness trends and climate drivers, particularly highlighting the dominant role of increased precipitation in driving the observed greening. Trend analysis reveals that while rain use efficiency (RUE) remains stable in most areas, increases in the NGP region suggest potential CO_2 fertilization effects, while decreases in southern states correlate with rising temperatures. We also develop an efficiency-based model featuring RUE which successfully reproduces historical NDVI, re-confirming the dominant influence of precipitation in local greenness interannual variability. However, CMIP6 projections for 2021–2040 under the 'Regional Rivalry' scenario (SSP370) paint a worrying picture, with projected browning in the NGP region and states near the 42°N latitude, contrasting recent greening trends. This potential reversal underscores the vulnerability of these ecosystems to future climate change, highlighting the need to consider both historical trends and future climate projections when assessing the resilience of drylands ecosystems. Overall, our work re-emphasizes the significance of water availability to drylands vegetation growth and contributes to a more comprehensive understanding of carbon-water cycling in arid and semi-arid regions.

1. Introduction

Dryland ecosystems play a critical role in the global carbon cycle, strongly contributing to the trend and inter-annual variability of the global terrestrial carbon sink, due to their high sensitivity to inter-annual climate variability (Ahlström *et al* 2015). Drylands feature a scarcity of water and are particularly susceptible to climate change (Lian *et al* 2021), especially variations in precipitation and temperature. Recent studies indicate declining future of water availability in drylands as climate projections show that drylands will experience increased warming, drought frequency, and evaporative demand at rates faster than the global average (Feng and Fu 2013, Lehner *et al* 2017, Bradford *et al* 2020, Müller and Bahn 2022). Drylands tend to be more severely impacted by drought events which stress local vegetation and subsequently affect their carbon sequestration capabilities. Conversely, as droughts exacerbate due to global

© 2025 The Author(s). Published by IOP Publishing Ltd

warming, the increasing level of CO_2 concentration is reported to benefit photosynthesis through the CO_2 fertilization effect (CFE) (Gonsamo *et al* 2021), as vegetation can keep their stomata closed for longer durations to conserve water for photosynthesis while maintaining a consistent level of intercellular CO_2 concentration (Zhang *et al* 2022).

Discrepancies between global and regional scale studies regarding the present trajectories of drylands are evident. Several analyses have indicated a global increase in aridity within drylands, resulting in significant and sudden alterations in numerous ecosystem characteristics (Berdugo *et al* 2020). A considerable portion of drylands has been reported to experience desertification and soil deterioration due to unsustainable land management practices exacerbated by human-induced climate variations (Burrell *et al* 2020). However, these assertions have been challenged with claims that conventional aridity metrics inadequately represent the land-based water cycle, thereby producing questionable outcomes from dynamic global vegetation models (Berg and McColl 2021). In contrast, trends of greening and increased vegetation activity across diverse dryland environments have been reported in regional studies (Hänke *et al* 2016, He *et al* 2019, Li *et al* 2022). Various factors contribute to this discrepancy in findings, with differing spatial resolutions of input datasets emerging as a pivotal factor. Coarse-resolution pixels consist of mixed land surface signals, leading to ambiguity in temporal trend analyses when compared with outcomes derived from datasets at finer resolution (Ji and Brown 2022, Zhang *et al* 2023). Spatial grain needs to be explicitly considered in dryland ecosystem which is constrained by precipitation when examining the influence of climate variables on local vegetation dynamics as experiments have shown that the effects of precipitation manipulation on plants are strongest at the smallest spatial scale compared to other environmental factors (Korell *et al* 2021).

Drylands in the conterminous United States (CONUS) account for more than 40% of the territory, encompassing a diverse array of arid and semi-arid ecosystems. These regions, including parts of the Great Basin, the Colorado Plateau, the Sonoran and Mojave Deserts, and most of the Great Plains, exhibit pronounced climatic variability. This climatic regime leads to a persistent water deficit, exerting a significant influence on soil moisture availability and vegetation dynamics. The temperature profiles in these regions are marked by extreme seasonal and diurnal variations. The high variability in temperature and precipitation, both spatially and temporally, underpins the ecological processes and biotic adaptations in these arid landscapes.

Few research endeavors have been focused on exploring the prolonged alteration in vegetation over an extensive time-frame in conjunction with contemporary climate fluctuations within CONUS on a continental scale, among global and site-specific investigations. This research addresses this gap by examining greenness trends in the natural CONUS drylands from 2001 to 2020, utilizing long-term satellite-derived normalized difference vegetation index (NDVI) data from MODIS. This study delves into the primary climatic drivers at 1 km spatial resolution through regression-based attribution and empirical orthogonal function (EOF) analysis, assessing associations from both temporal and spatial perspectives. To evaluate the local ecosystem's functionality, adaptability, and reaction to climatic changes, the study specifically scrutinizes the long-term trends of rain use efficiency (RUE) across the entire research area. Furthermore, we develop a simplified model based on RUE to replicate observed NDVI trends and annual variations, projecting NDVI alterations in CONUS drylands for the subsequent two decades (2021–2040) utilizing downscaled CMIP6 precipitation projections.

2. Data and methods

2.1. Terra MODIS vegetation index products

The NDVI observations in this study comes from Terra MODIS Vegetation Index Products Collection 6.1 (MOD13Q1 v061) (Didan 2021, DOI: https://doi.org/10.5067/MODIS/MOD13Q1.061) which provides consistent, spatial, and temporal comparisons of global terrestrial vegetation conditions. NDVI is provided as 16 d composite layers at 250 m spatial resolution. To maintain the consistency of the data sources across all years, only Terra MODIS products are used to acquire NDVI observations for its longer record compared to Aqua products. Only data for 2001–2020 is used. In addition, to exclude the effects of cloud cover, surface reflectance inconsistences, and other potential artifacts, we mask out pixels related to bad quality according to the built-in VI Quality band. We also adopt a upward-smoothing approach to fill the data gap (Chen *et al* 2004).

2.2. MODIS land cover (LC) type products

The LC type information is obtained from MODIS Terra and Aqua combined LC Type products Collection 6.1 (MCD12Q1 v061) (Friedl and Sulla-Menashe 2022, DOI: https://doi.org/10.5067/MODIS/MCD12Q1.061) which provide global LC types at yearly intervals from 2001 to 2022. The spatial resolution of MCD12Q1 is 500 m. This study specifically uses the International Geosphere-Biosphere Programme classification scheme. To focus on vegetation change in natural drylands and avoid influence of human intervention, pixels classified as one of following four LC types, Croplands, Urban and Built-up Lands, Cropland/Natural Vegetation Mosaics (Semi-Croplands), and Water Bodies, in any LC layers within

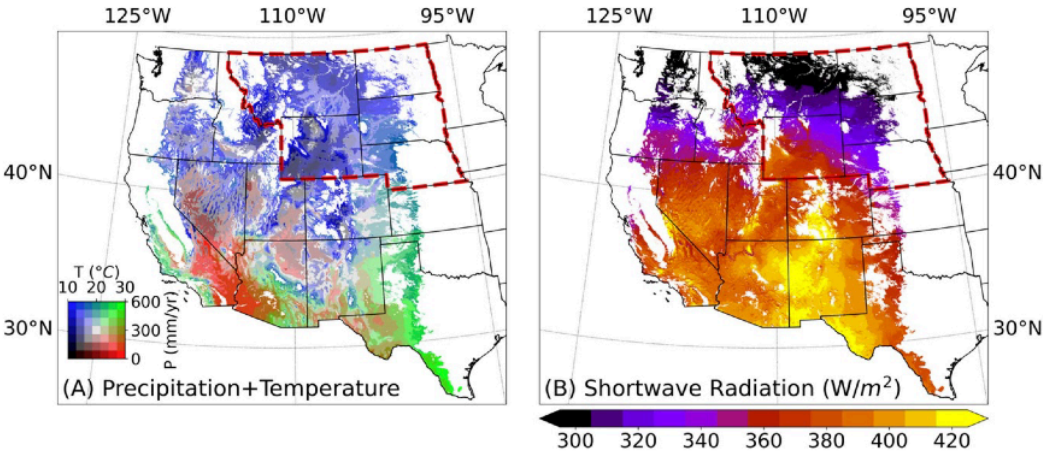

Figure 1. Climatology (2001–2020) spatial distribution of climate drivers in CONUS drylands (ATP < 600 mm yr^{-1}). The enclosed area defines the zoom-in study region in the northern Great Plains. (A) Joint spatial distribution of annual total precipitation and annual mean daily maximum temperature. Distinct regional patterns can be observed; (B) spatial distribution of daytime incident shortwave radiation flux density. Its value varies mainly along latitude.

the two-decade study period are further masked out. To maintain spatial gridding consistency across datasets, the final decision is made on a resampled 1 km reference LC composite map.

2.3. Meteorological data

Data of precipitation, daily maximum temperature, and incoming shortwave radiation flux density used in this study are collected from Daymet: Daily Surface Weather Data (Version 4) (Thornton *et al* 2022, available at https://doi.org/10.3334/ORNLDAAC/2129). This dataset offers persistent and continuous gridded estimations of daily weather and climatological variables at 1 km spatial resolution and over an extended period (1980–2022), which is arguably the most accurate and updated meteorological dataset currently available for CONUS. These estimations are derived by interpolation and extrapolation of ground-based observations through statistical modeling techniques (Thornton *et al* 2021).

2.4. Study region

This study focuses on CONUS drylands, defined as areas receiving less than 600 mm of annual total precipitation (ATP). Figure 1 illustrates the spatial patterns of key climate variables across the study region, highlighting distinct regional differences. Precipitation tends to be the primary limiting factor for vegetation growth in CONUS drylands, particularly in the south (Nemani *et al* 2003). While temperature exerts a secondary influence, its importance increases with latitude. This is reflected in the three distinct climate zones evident in figure 1(A): the northern Great Plains (NGP) region, encompassing Montana, Wyoming, North Dakota, South Dakota, and Nebraska, is characterized by a relatively wet and cool environment and is the focus of further investigation in this study; the Southern Great Plains have a wet and hot climate; and the Southwestern states are dominated by dry and hot conditions. Figure 1(B) further reveals the spatial distribution of incoming shortwave radiation, which exhibits variation primarily along latitudinal gradients.

2.5. Temporally summarized datasets

The primary challenge of analyzing the impacts of interdependent and correlated climatic factors on the trend of greenness is to identify climate indices that effectively capture the 'period of climatic influence' (Ahlström *et al* 2015). Because of that, two types of datasets, annual and growing season summarized datasets, are created for NDVI and three climatic variables from original monthly datasets. Annual summarized data has the merit of being simple and is more useful for studying extensive areas where heterogeneity in growing seasons is present. Growing season summarized data is in general a better proxy for quantifying the direct influence of climatic variables on vegetation growth. By adopting growing season identifying methods introduced in Körner *et al* (2023), a period of six months (April–September) is determined as the growing season (monthly resolution) for the NGP region (figure S1). Corresponding growing season average/sum datasets are created for all variables.

2.6. Trend analysis

In this study, trends are evaluated using the Mann–Kendall (MK) test, a non-parametric method well-suited for detecting trends in vegetation indices without assuming data normality (de Jong *et al* 2011, Fensholt *et al* 2012, Chen *et al* 2019). Specifically, we employ the modified pre-whitening MK test

(Yue *et al* 2002), which reduces potential false positives by mitigating autocorrelation in time series data. For computational efficiency, the pyMannKendall package (Hussain and Mahmud 2019) source code is adapted for compatibility with C++. A significance level (α) of 0.1 is set, indicating that a time series with $p \leqslant 0.1$ exhibits a statistically significant trend.

2.7. Empirical linear attribution method

A multiple linear regression (MLR) model is employed to attribute observed greenness changes to the dominant climate drivers. MLR has been adopted in studying spatial-temporal variation of LAI (Zhang *et al* 2024), soil properties (Forkuor *et al* 2017), and droughts (Kim *et al* 2020). Similar methods are used to assess contributions of anthropogenic and natural factors to global climate change (Lean and Rind 2008, Canty *et al* 2013, Stern and Kaufmann 2014). The regression coefficients in MLR provide conceptually simple and direct measures of magnitude and direction of the relationship between NDVI and each climate variable, allowing a straightforward assessment of the relative contributions of different drivers. This approach assumes predictor independence. To ensure this, the correlation matrix is evaluated prior to analysis. The model takes the following form:

$$\Delta V = \alpha + \beta_1 \Delta P + \beta_2 \Delta T + \beta_1 \Delta R_{\mathrm{sw}} + \in \qquad (1)$$

where the Δ terms are normalized anomalies of each variable, β_i is the associated coefficient, α is the intercept, and $\in$ is the error term, and V, P, T and R_{sw} denote greenness (NDVI in this study), precipitation, temperature, and shortwave radiation, respectively.

Anomalies are calculated as deviations from climatological means, and normalization is achieved by dividing by the Euclidean (L2) norm. This allows each time series to be viewed as a unit vector in multidimensional space. By evaluating the coefficients, the interannual variability of NDVI in the study region can be attributed to its potential climate drivers.

2.8. EOF analysis

EOF analysis is commonly used to reduce the dimensionalities of the datasets and extract the leading modes of variability which are often assumed to relate to various physical processes (Volkov *et al* 2022). It has vast applications in environmental studies to analyze spatiotemporal patterns of climate variables (Zhang *et al* 1997, Roundy 2015, Tippett and L'Heureux 2020, Werb and Rudnick 2023). We employ EOF analysis in this study to assess the intercorrelation between NDVI and selected climate variables in both spatial and temporal domains. For each mode of a climate variable, a spatial regression map (EOF_i) and the corresponding principal component (PC_i) are generated, and they are then compared with the EOF analysis results of NDVI using different techniques. A python package (eofs) (Dawson 2016) is used for performing the analysis.

2.9. RUE and efficiency-based model

RUE refers to the ratio of Aboveground Net Primary Production (ANPP) to total precipitation, and it is an effective index for assessing ecosystem productivity of drylands (Le Houérou 1984). The linear relationship between ANPP and NDVI has been well studied and established (Myneni and Williams 1994, Holm *et al* 2003, Wessels *et al* 2006, Prince 2007, Rasmussen 2010, Xue *et al* 2017). Temporal integrated NDVI (ΣNDVI or iNDVI) is found to be a consistent proxy for ANPP (Chang *et al* 2018, Dardel *et al* 2014, Fensholt *et al* 2013, Kaptué *et al* 2015, Paruelo *et al* 1999). In this study, the temporal average NDVI ($\overline{\mathrm{NDVI}}$), which is conceptually equivalent to iNDVI (only differ by a constant factor), is used for RUE calculation,

$$\mathrm{RUE} = \frac{\overline{\mathrm{NDVI}}_n}{\sum_1^n P_i} \qquad (2)$$

where n represents the number of months, which varies depending on the period (annual or seasonal) for which the RUE is evaluated, and i denotes the month.

To rule out the climate influence on vegetation beyond the target period, which is often defined as the 'zero intercept' difficulty when using NDVI instead of ANPP for RUE calculation (Verón *et al* 2005, Dardel *et al* 2014). A concept of baseline average NDVI ($\overline{\mathrm{NDVI}}_b$) is proposed in this study. It is assumed to be proportionate to a portion of *in-situ* ANPP which is not attributable to the precipitation descended within the target period but rather to the stored soil moisture or underground water. $\overline{\mathrm{NDVI}}_b$ in this study is taken as the minimum monthly mean NDVI during a year for annual case, and the monthly mean NDVI over three non-growing season months prior to the growing season for seasonal case. The improved RUE calculation is then expressed as below,

$$\mathrm{RUE} = \frac{\overline{\mathrm{NDVI}}_n - \overline{\mathrm{NDVI}}_b}{\sum_1^n P_i} \quad . \qquad (3)$$

The regional average RUE is calculated as the ratio of pixel-wise sum of NDVI to the pixel-wise sum of total precipitation,

$$\overline{\mathrm{RUE}} = \frac{\sum_1^N \left(\overline{\mathrm{NDVI}}_{n,p} - \overline{\mathrm{NDVI}}_{b,p}\right)}{\sum_1^N \sum_1^n P_{i,p}}, \qquad (4)$$

where N denotes the pixel count of the target region, and p denotes the pixel index.

Based on RUE, we proposed a efficiency-based model to reproduce the historical NDVI interannual variability and project future conditions of CONUS drylands vegetation. This model is adapted from an open-loop linearized model, first introduced in

Wang *et al* (2006), which is established for semi-arid grassland regions in the North America to quantify the vegetation dynamics and contribution of precipitation to local vegetation growth. With the main difference that we aim to study vegetation change and its correlation with precipitation seasonally and annually instead of monthly in its original work, we can safely regard that NDVI can be informed by contemporary precipitation, given the prolonged study period and transit nature of precipitation in drylands environments. The modified model has the following form,

$$V_t = \alpha V_{b,t} + \beta P_t + \in_t \quad (5)$$

where V_t and $V_{b,t}$ denote the temporal average NDVI and corresponding baseline NDVI, α and β denote the persistence rate of greenness and RUE, respectively, P_t is the total precipitation of interested period.

To account for the widely observed negative correlation between RUE and precipitation (RUE decreases as precipitation increases) (Huxman *et al* 2004, Zhang *et al* 2020), RUE (β) in this model is calculated as the sum of its climatology value and response to precipitation anomaly (ΔP) by coefficient k, which has the following form,

$$\beta = \beta_0 \cdot (1 + k\Delta P_t) \ . \quad (6)$$

When $V_{b,t}$ is taken as its climatology value, the only independent variable in this model is annual or seasonal total precipitation.

2.10. Future projections from downscaled CMIP6 simulations

The proposed efficiency-based model is further used for projecting the future greenness conditions of CONUS drylands, with the state-of-the-art CMIP6 climate projections as inputs (Eyring *et al* 2016). WorldClim (worldclim.org) provides the latest downscaled CMIP6 projections at 30 arc seconds, processed and calibrated with WorldClim v2.1 (Fick and Hijmans 2017) as baseline climate. 20-year climatology monthly precipitation predictions for the future (2021–2040) are obtained from six global climate models (GCMs), GFDL-ESM4 MIROC6, MPI-ESM1-2-HR, EC_Earth3-Veg, UKESM1-0-LL, and CMCC-ESM2, for the boundary conditions given by the SSP370 scenario (O'Neill *et al* 2016). SSP370 is specifically selected because the projection period (2021–2040) is not far into the future. Because of that, we predict the trajectory of our study region, assuming that there is no major change in the environment policies for the next two decades. SSP370 is the one closest to the 'business as usual' scenario among all available SSPs.

3. Results and discussions

3.1. Inter-annual NDVI trend and relationship with climate drivers

The 20 year trend analysis of annual mean NDVI in CONUS drylands (figure 2(A)) reveals a predominance of non-significant trends, with the notable exception of the NGP region, which exhibits extensive and clustered greening. In other states, significant greening trends are fragmented and sparsely distributed. Arizona also demonstrates notable greening trends, though less pronounced than in the NGP and weaker in magnitude. Browning trends are minimal across the study area, occurring primarily at a micro-scale, with slightly higher prevalence in New Mexico and west Texas. Focusing on the NGP region, figure 2(B) illustrates the growing season mean NDVI trend, revealing a larger proportion of pixels with increasing trends compared to the annual mean NDVI analysis. Figure 2(C) compares the time series of annual mean NDVI for all CONUS drylands with the seasonal mean NDVI of greening pixels in the NGP. As confirmed by the MK test, the annual mean NDVI of all dryland pixels shows no significant trend over the study period due to the relatively small proportion of greening pixels. In contrast, within the NGP region, the seasonal mean NDVI of greening pixels exhibits a consistent and steady increasing trend despite clear interannual variability. Figure S2 shows the LC map for CONUS drylands. Grasslands dominate CONUS drylands (71%), followed by shrublands (17%), together comprising nearly 90% of the area. Greening trends are evident in 16% of the study area, concentrated primarily in the NGP grasslands (90% of the greening trend). Browning trends are minimal (1%).

Climate variables exhibit varied trend patterns in the CONUS drylands (figure 3). Among all three climate factors, precipitation is most strongly correlated with greening trends in CONUS drylands, especially in the NGP region. While some spatial inconsistencies exist, the association between increased precipitation and vegetation greening is clear. Temperature appears to be less influential, and shortwave radiation exhibits a minor negative correlation with greening. Outside the NGP region, precipitation trends are less significant, while positive temperature trends are observed in southern California, Arizona, New Mexico, and Texas. To understand the drivers of the significant greening trend in the NGP region, the MLR model is applied to greening pixels only. Analysis revealed weak but negligible correlation between climate variables, validating the variable independence assumption (figure S3). The model effectively reproduced observed NDVI patterns (R-squared = 0.685) (figure S3). Table 1 shows the values of coefficients from the attribution analysis. Precipitation is the dominant driver, with a significantly larger coefficient (0.8001) compared

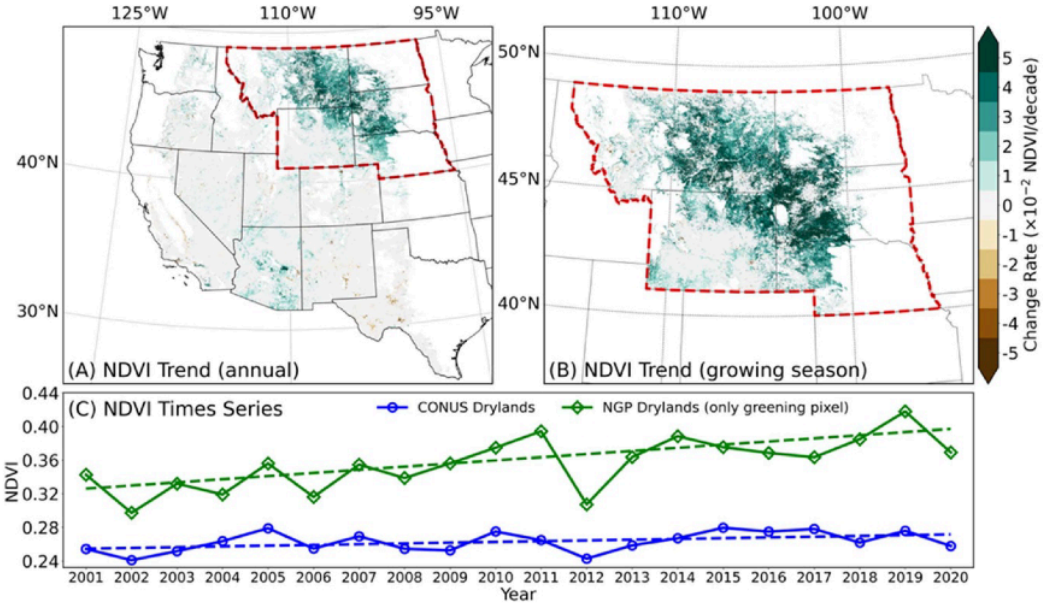

Figure 2. Results of NDVI trend analysis from 2001 to 2020. (A) Annual mean NDVI trend in CONUS drylands; (B) growing season mean NDVI in the northern Great Plains (NGP) region; (C) zonal-average NDVI time series for two regions of interest. The blue line represents the annual mean NDVI averaged over all pixels in CONUS drylands. The green line represents the growing season mean NDVI averaged over only greening pixels (P-value < 0.1) in NGP drylands. The dashed lines are fitted regression lines according to MK test. The green line shows significant increasing trend (P-value < 0.1). The blue line does not show any significant trend.

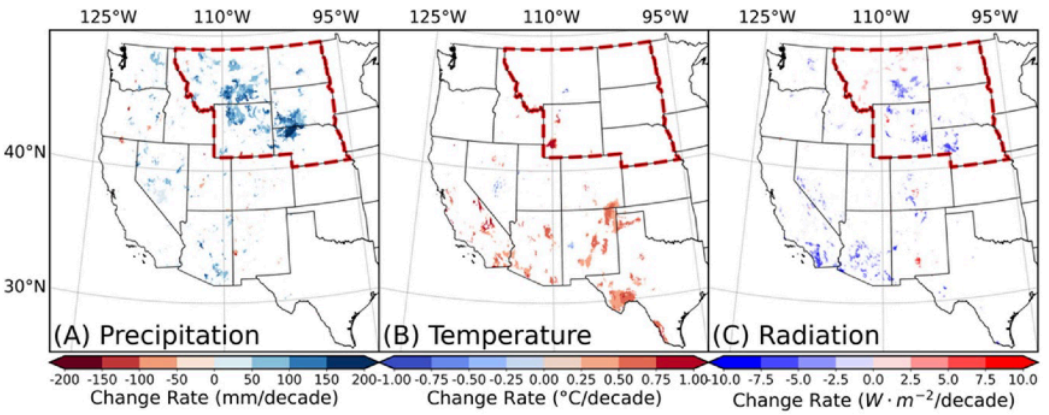

Figure 3. Trends of climate variables from 2001 to 2020. (A) Annual total precipitation; (B) daily maximum temperature; (C) shortwave radiation flux density.

Table 1. Results of the empirical linear attribution model.

Coefficient	Value	P-value
α	<0.01	1
β_1	0.8001	0.037
β_2	0.0169	0.939
β_3	−0.0455	0.877

Note: α is the intercept term in the MLR model. Its close-to-zero value indicates the selected climate variables explain the most variability in NDVI anomalies. β_1, β_2 and β_3 are coefficients corresponding to anomalies of precipitation, temperature and shortwave radiation.

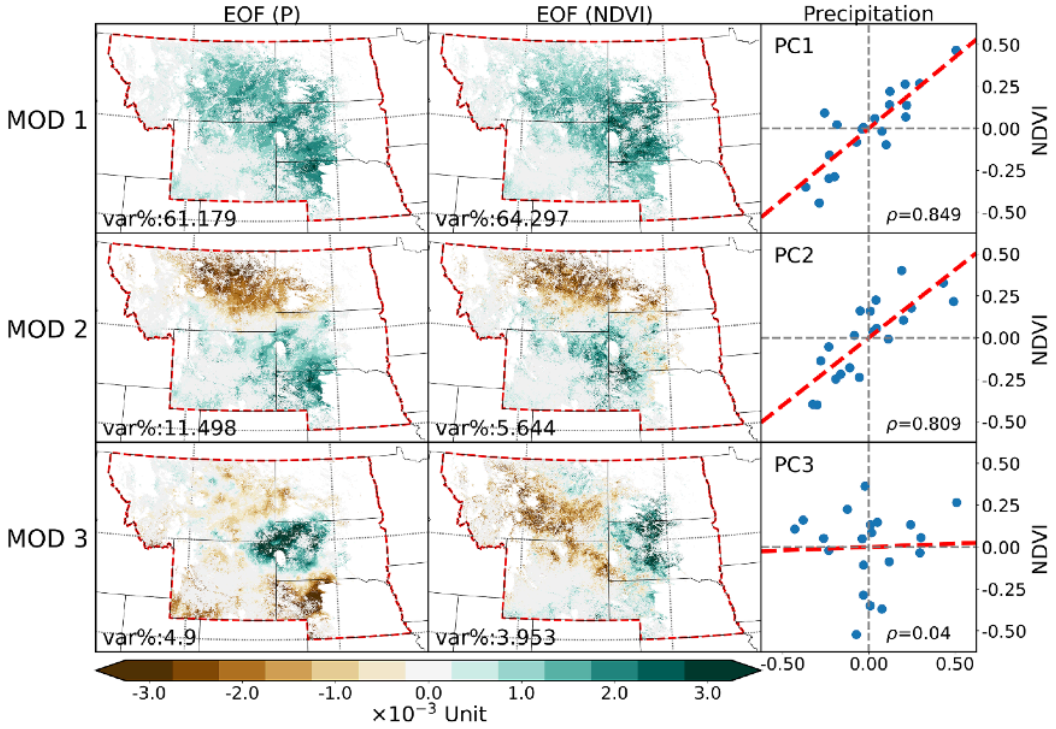

Figure 4. EOF analysis of seasonal precipitation and NDVI anomalies from 2001 to 2020. Only the results of the first three leading modes (EOF) and corresponding principal components (PC) for each variable are presented. The first two columns present the EOFs, and the third column presents the comparison of corresponding PCs.

to temperature and radiation whose coefficients are close to zero (0.0169 for T, −0.0455 for R_{sw}), indicating minimal influence on the observed NDVI interannual variability. This highlights the importance of precipitation in driving vegetation greening in the NGP region. The comparison of the interannual variability of NDVI and precipitation is provided in figure S6.

EOF analysis is conducted to further investigate the relationship between precipitation and NDVI in the NGP region, following the attribution model results. Figure 4 shows the EOF analysis results. The first two EOF modes of both precipitation and NDVI capture the majority of the variance (72.7% and 69.8%, respectively), exhibiting similar spatial patterns and a high correlation ($\rho = 0.849$) between their PCs. This confirms that interannual variability in seasonal NDVI is primarily driven by local precipitation, with no lagged effects. The first EOF mode for each variable also aligns with the spatial patterns observed in the trend analysis. The second EOF modes, while still highly correlated ($\rho = 0.809$), reveal a latitudinal gradient in both precipitation and NDVI, suggesting the influence of other latitude-dependent climate factors on plant growth. However, the direct driver remains precipitation. From the third mode onwards, spatial correlations decrease significantly. The third EOF modes for precipitation and NDVI present similar regional clusters. This might indicates a weak topographic link between precipitation and NDVI variability at finer spatial scales.

Based on the combination of historical precipitation records and earth observations, precipitation in CONUS drylands is surely experiencing spatial shifting. Precipitation has become more unevenly distributed over the two-decade study period. Water availability in northern states, especially the NGP region, are progressively improved as the result of increase in precipitation, which theoretically increases the capacity of corresponding area to sustain denser and higher-level vegetation communities. In contrast, water scarcity for vegetation growth is expected to intensify in the southern states, including southern California, Arizona, New Mexico, and western Texas, mainly due to the widely observed increase in air temperature (Wahl *et al* 2022, Zhuang *et al* 2024). The local potential evapotranspiration becomes even higher because of the elevated vapor-pressure deficit (Swain *et al* 2025), which strengthens the water constraint on local plant growth.

3.2. RUE patterns and CFE

Analysis reveals a significant linear relationship between precipitation and NDVI in our study regions over the two-decade period, evident from both annual (figures S4&S5) and climatological perspectives (figures 5(A) and (B)). Strong

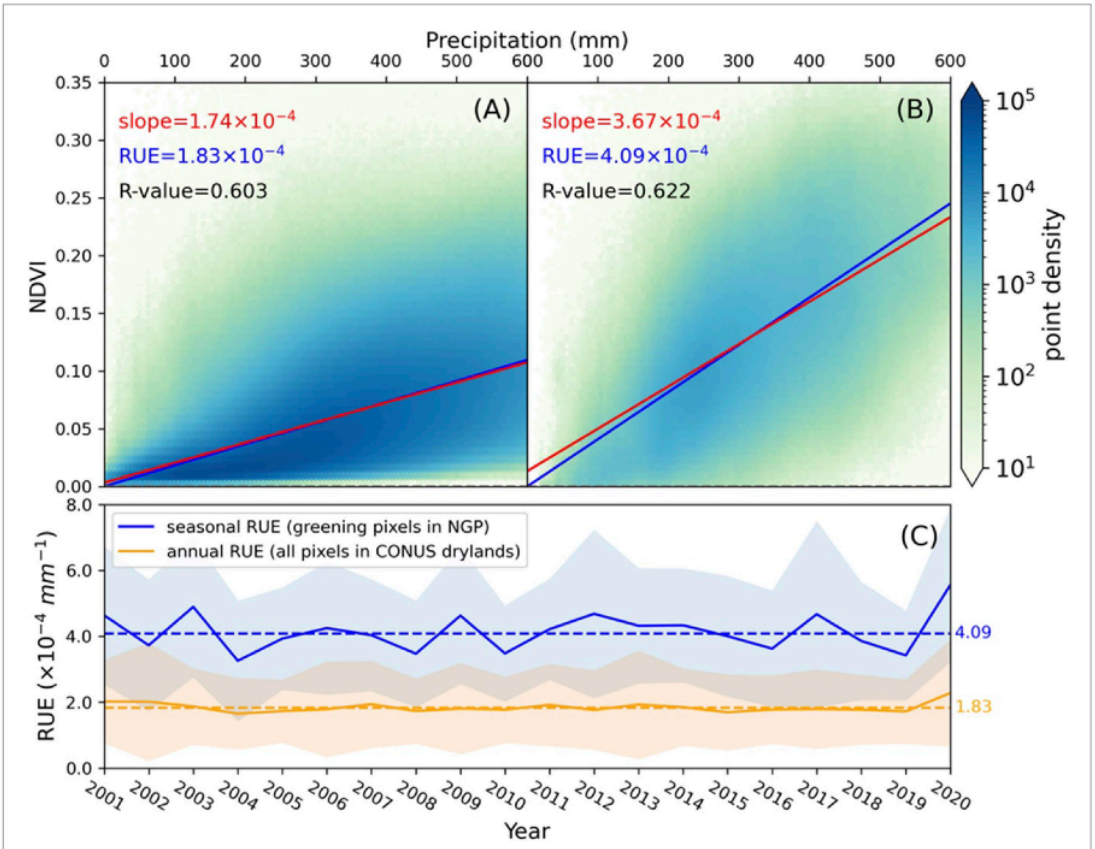

Figure 5. Rain use efficiency in the CONUS drylands and NGP region. (A) Scatter plot of climatology annual mean NDVI against annual total precipitation (ATP) in the CONUS drylands; (B) scatter plot of climatology growing season mean NDVI against growing season total precipitation for greening pixels only in the NGP region; (C) time series comparison of yearly annual mean RUE in CONUS drylands (orange line) and seasonal mean RUE in the NGP region (blue line, greening pixels only). The shading represents one standard deviation interval for each line. No trend is detected for both RUE time series by MK test ($\alpha = 0.1$).

correlations (> 0.6) between climatological NDVI and precipitation suggest a stable long-term mean RUE, around which yearly values fluctuate. The wide shading areas (one standard deviation interval) in figure 5(C) highlight substantial spatial variation in RUE, likely due to varying species composition and local environmental factors. Despite this variability, MK tests detect no significant RUE trends from 2001 to 2020 at the aggregated spatial scale (figure 5(C)). Per-pixel trend analysis of RUE reveals greater spatial variation. While most pixels show no trend (figure 6(A)), a significant number of pixels in the NGP region exhibit increasing annual mean RUE, largely coinciding with areas of increasing precipitation and NDVI. Although spatial discrepancies exist, annual and seasonal RUE trends in this region show broad similarity (figures 6(A) and (B)). Notably, clusters of increasing seasonal RUE are concentrated further downstream along the Missouri River, compared to annual RUE. Outside the NGP region, increasing RUE is sparsely distributed, primarily along the 40°N latitude. Further south, declining RUE becomes more prevalent, particularly in southern California bordering Arizona, New Mexico, and Texas. This pattern of decline spatially overlay the increasing temperature trends in figure 3(B).

While a negative relationship between precipitation and RUE is often observed due to reduced water limitation (Huxman *et al* 2004, Chen *et al* 2020), the NGP region exhibits a contrasting pattern of increasing RUE alongside increasing precipitation. This suggests factors beyond simple water availability are at play. In drylands, high potential evapotranspiration and sparse vegetation can limit the translation of increased precipitation into significant improved plant growth (and RUE) (Zhu *et al* 2022). A growing body of research has revealed the large-scale CFE in drylands (Uddin *et al* 2018, Rifai *et al* 2022, Verbruggen *et al* 2024). It has been commonly accepted that CFE increases water use efficiency (WUE) through reducing stomatal conductance (Haverd *et al* 2020). This phenomenon is expected to be more prominent in water limited areas, such as drylands, as local vegetation tends to save water while maintaining the level of photosynthesis. The observed RUE increase in the NGP region (figures 6(A) and (B)) further highlights CFE as a key driver (Gonsamo *et al* 2021, Zhang *et al* 2022). CFE in cool grasslands is also

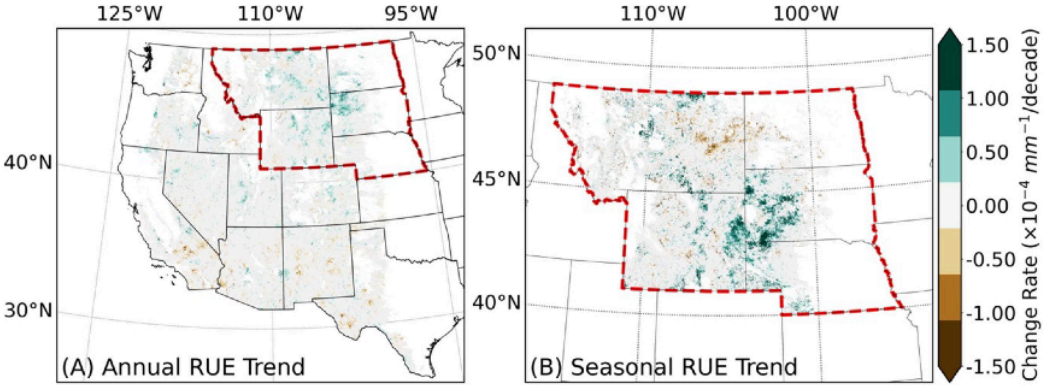

Figure 6. Per-pixel rain use efficiency trend analysis results. (A) Trend of annual mean RUE in the CONUS drylands; (B) trend of seasonal mean RUE in the NGP region.

echoing findings in Winkler *et al* (2021). However, in contrast to expected large-scale increases in RUE across CONUS drylands due to CFE, figures 6(A) and (B) show that significant increases in RUE are limited to areas with concurrent increases in precipitation (figures 8(C) and 9(A)). This highlights the complex interplay between water availability and CFE in driving vegetation dynamics in response to climate change in drylands.

If specifically considering the role of plant transpiration in RUE calculation, equation (2) can be rewritten as follow,

$$\mathrm{RUE} = \frac{\overline{\mathrm{NDVI}}}{\sum P} = \frac{\overline{\mathrm{NDVI}}}{\sum E_T} \cdot \frac{\sum E_T}{\sum P}. \tag{7}$$

The increase in atmospheric CO_2 concentration affects plant growth in two major ways, reducing stomata conductance ($\frac{\sum E_T}{\sum P}$) by shortening the duration of stomata opening and stimulating vegetation cover ($\frac{\overline{\mathrm{NDVI}}}{\sum E_T}$). Zhang *et al* (2022) concluded that the increase in sensitivity of dryland vegetation greenness to precipitation is mainly because the stimulation effect overrides the decline in $\frac{\partial E_T}{\partial P}$ in those ecosystems. In our study region, except the NGP region, the simulation effect is limited as indicated by the relatively unchanged NDVI. The WUE ($\frac{\overline{\mathrm{NDVI}}}{\sum E_T}$) of local plants may have increased so that it compensates for the decrease in stomata conductance, but not to the point where the RUE also shows significant changes.

The above explanation assumes that vegetation in drylands aims to maximize WUE and that CFE suppresses stomatal conductance, consistent with the traditional optimality theory of plants (Cowan and Farquhar 1977). However, Wolf *et al* (2016) propose that under conditions of intense water competition—driven by high evaporative demand and competition from neighboring plants—a more evolutionarily advantageous strategy for plants may be to prioritize growth rate by keeping stomata open, even at the cost of reduced WUE. The absence of a large-scale increase in RUE and the spatially correlated increase in RUE with precipitation in the NGP region (figures 6(A) and (B)) supports this theory at the ecosystem scale. This suggests that alleviating water limitations could be a prerequisite for dryland ecosystems to fully benefit from elevated CO_2 concentrations. To reach a decisive conclusion requires a thorough quantitative analysis of the long-term stomatal behavior of local vegetation, accounting for the plant hydraulic stress imposed by scare soil moisture in drylands.

The similarity in the spatial distributions of the decreasing RUE and increasing temperature patterns observed in the southern states implies their physiological connections. The influence of temperature on RUE is complicated, as optimum temperature ranges exist for all biomes, in which vegetation balances it carbonate production and water loss through stomata. Drylands in southern states are characterized by excessive temperature and dry environments. Increasing temperature in water limited region strengthens the need of plant to preserve water through further reducing the stomata conductance. As a result, the intensified reduction of $\frac{\sum E_T}{\sum P}$ entails the observed decrease in RUE in southern states.

3.3. Modeling and projections

The proposed model aims to quantify the interannual variability of NDVI in CONUS drylands using precipitation as the sole independent variable. Model performance is evaluated across both temporal and spatial domains. We first use the model to reproduce the time series of observed spatial-average NDVI for two regions: the NGP region (using growing season mean NDVI) and the entire CONUS drylands (using annual mean NDVI). As presented in table 2, there are 61 888 211 and 16 742 453 valid pixels in total used for parameter estimation in two different cases. Their respective R-squared values are 0.721 and 0.859, indicating good model fit. The estimated climatological RUE (β_0) (table 2) closely match values derived directly from the data (figure 5(C)). Figure 7 further demonstrates strong agreement between observed

Table 2. Modeling results in two study regions.

Results	Region	
	NGP	CONUS
# of pixels	16 742 453	61 888 211
R^2	0.721	0.859
Intercept	−0.009	−0.011
α	0.966	1.037
k	-2.620×10^{-7}	-7.220×10^{-8}
β_0	4.721×10^{-4}	1.970×10^{-4}

Note: α, k, and β_0 in the above table are estimated parameters, representing the persistence rate of greenness, the sensitivity of RUE to precipitation anomaly, and climatology RUE.

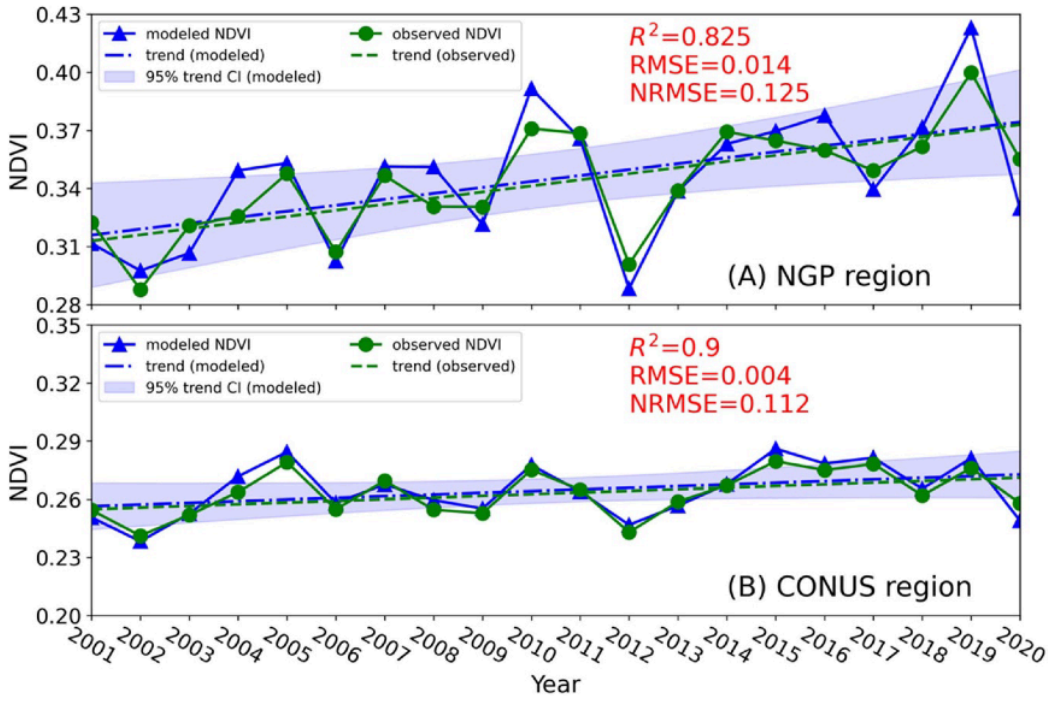

Figure 7. Comparison of observed and modeled NDVI interannual variability in (A) NGP and (B) CONUS dryland regions. The trend lines for observed and modeled NDVI, as estimated through linear regression in both panels, exhibit a high degree of overlap. Significant increasing trends are detected in both observed and modeled in (A) by MK test. No significant trends are detected in (B) by MK test.

and modeled spatial-average NDVI times series over time. The model effectively reproduces the spatial-average NDVI time series in both regions, exhibiting high R^2 values (0.825 for NGP and 0.9 for CONUS), low RMSE (0.014 and 0.004), and low NRMSE (0.125 and 0.112). These results confirm the model's ability to capture the temporal dynamics of NDVI. To assess the model's ability to capture spatial heterogeneity, we applied it at the pixel level across the entire study region (figure 8). R^2 values exceed 0.5 for most pixels (figure 8(A)). Excluding pixels with insufficient data or invalid parameters, the relative error between modeled and observed climatological annual mean NDVI remains below 10% for most areas, with some overestimation (around 10%) observed in the NGP region (figure 8(B)). Overall, the proposed model demonstrates robust performance in capturing the interannual variability of NDVI in CONUS drylands, both temporally and spatially, underscoring the critical role of water availability in driving vegetation dynamics.

The model's success in reproducing observed NDVI patterns validates its utility for understanding and predicting vegetation responses to precipitation variability, particularly in light of future CMIP6 projections that indicate a potential reversal of recent greening trends. These projections, based on averaging predictions from six different models (GFDL-ESM4 MIROC6, MPI-ESM1-2-HR, EC_Earth3-Veg, UKESM1-0-LL, and CMCC-ESM2) under the SSP370 scenario, show a widespread decrease in climatological ATP of approximately 20% in the NGP

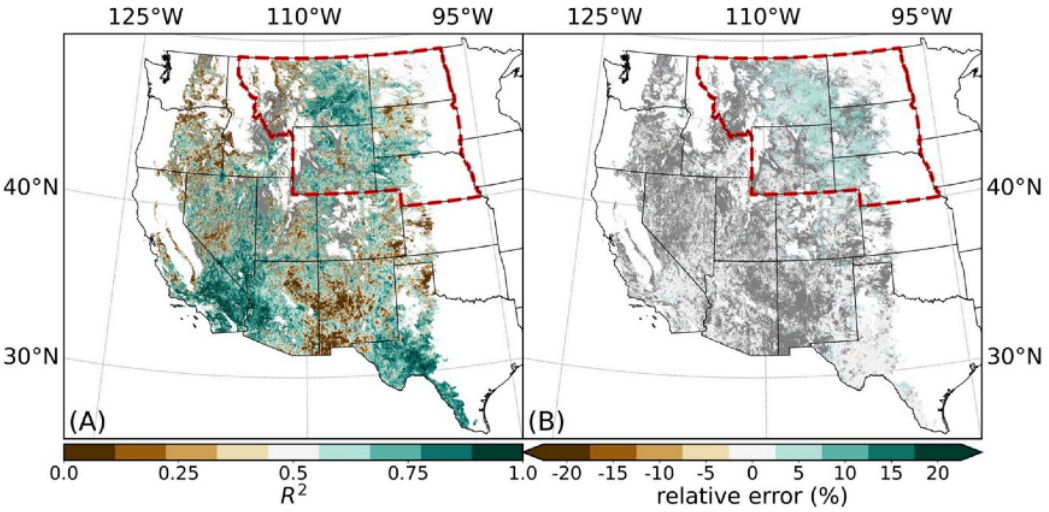

Figure 8. Per-pixel modeling results in the CONUS drylands. (A) Presents the coefficient of determination (R^2) at each pixel; (B) presents the relative error between observed and modeled climatology annual mean NDVI (2001–2020) in percentage. Shaded area (gray) in (A) represents masked pixels which have less than 15 valid NDVI observations out of 20 years. Shaded area (gray) in (B) represents masked pixels that combine the shaded area in (A) and pixels with R^2 lower than 0.5 or negative estimated β_0 (RUE).

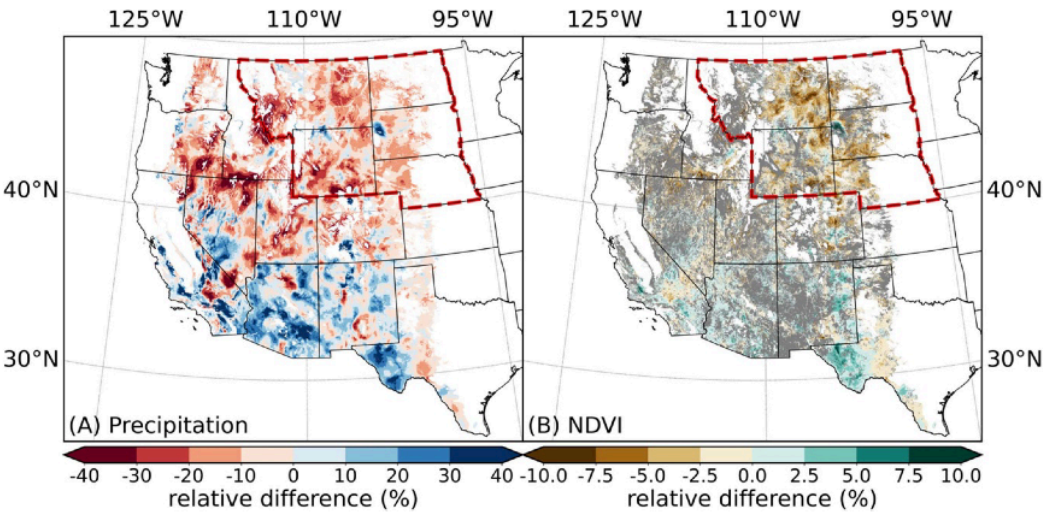

Figure 9. Relative differences between (A) climatology annual total precipitation of the study period (2001–2020) and CMIP6 climatology projection (2021–2040), and (B) climatology NDVI of the study period and projected NDVI estimated by per-pixel model, using CMIP6 climatology precipitation projection (2021–2040) as input. Shaded area (gray) in (B) represents masked pixels in figure 8(B). CMIP6 climatology precipitation projection is taken as the average of precipitation simulations of different GCMs under SSP370 scenario.

region (figure 9(A)), with corresponding declines in NDVI of up to 10% (figure 9(B)). This potential browning trend, contrasting with the observed greening, could have significant implications for ecosystem services and carbon sequestration in the NGP and Midwest. While some southern states may experience localized vegetation increases due to increased precipitation, the limited extent of these areas underscores the overall vulnerability of CONUS drylands to future climate change.

It is important to acknowledge that these projections rely on simplified assumptions and do not account for potential shifts in vegetation communities or factors like CFE. While demonstrating strong predictive power, the model's reliance on precipitation as the sole predictor also highlights a potential limitation. Future research should incorporate additional variables, such as temperature and soil moisture, to enhance its accuracy and applicability.

4. Conclusion

This study utilizes 20 year MODIS NDVI data and high-resolution meteorological data (1 km) to analyze long-term vegetation changes in CONUS drylands and their responses to climate variability. We find substantial greening trends across the NGP region from 2001 to 2020, primarily driven by increased precipitation. Temperature and shortwave radiation exert secondary influences on NDVI by modulating local precipitation patterns. While rising CO_2 appears to enhance RUE in NGP region where increasing trends of precipitation is also present, decreases in RUE across southern states correlate with rising temperatures, highlighting the complex interplay of climate factors on vegetation. Although CFE is expected to promote vegetation growth in drylands by enhancing water-use efficiency, the extent of this effect depends on local environmental conditions, particularly water availability, which is in contrast with large-scale CFE in drylands concluded in studies using coarser resolution products. These discrepancies also suggest the important role of stomatal behavior in understanding the adaptation of vegetation in drylands to changing climate. Our efficiency-based model effectively quantifies NDVI variability, emphasizing the critical role of water availability in dryland ecosystems. However, CMIP6-based projections using this model suggest potential future browning in the NGP region and areas near 42°N latitude, contrasting with recent greening trends. This underscores the vulnerability of these ecosystems to future climate change, although adaptive capacity and human interventions may modulate these outcomes. Our findings highlight the need for adaptive management strategies to mitigate potential negative impacts on dryland vegetation and emphasize the importance of incorporating additional factors into future models for enhanced accuracy.

Data availability statement

All data that support the findings of this study are included within the article (and any supplementary files).

Acknowledgments

The authors acknowledge funding from NASA Earth Science Division to Boston University under the MODIS (9500312733) and VIIRS (9500312663) Programs.

Conflict of interest

The authors declare no conflict of interests.

ORCID iDs

Yuhe Chang https://orcid.org/0009-0001-5218-2526
Alexander J Winkler https://orcid.org/0000-0001-6574-4471
Amirhossein Noori https://orcid.org/0009-0005-7546-7494
Yuri Knyazikhin https://orcid.org/0000-0002-3116-5719
Ranga B Myneni https://orcid.org/0000-0002-0234-6393

References

Ahlström A *et al* 2015 The dominant role of semi-arid ecosystems in the trend and variability of the land CO_2 sink *Science* **348** 895–9
Berdugo M *et al* 2020 Global ecosystem thresholds driven by aridity *Science* **367** 787–90
Berg A and McColl K A 2021 No projected global drylands expansion under greenhouse warming *Nat. Clim. Change* **11** 331–7
Bradford J B, Schlaepfer D R, Lauenroth W K and Palmquist K A 2020 Robust ecological drought projections for drylands in the 21st century *Glob. Change Biol.* **26** 3906–19
Burrell A L, Evans J P and De Kauwe M G 2020 Anthropogenic climate change has driven over 5 million km^2 of drylands towards desertification *Nat. Commun.* **11** 3853
Canty T, Mascioli N R, Smarte M D and Salawitch R J 2013 An empirical model of global climate—part 1: a critical evaluation of volcanic cooling *Atmos. Chem. Phys.* **13** 3997–4031
Chang J, Tian J, Zhang Z, Chen X, Chen Y, Chen S and Duan Z 2018 Changes of grassland rain use efficiency and NDVI in Northwestern China from 1982 to 2013 and its response to climate change *Water* **10** 1689
Chen C *et al* 2019 China and India lead in greening of the world through land-use management *Nat. Sustain.* **2** 122–9
Chen J, Jönsson P, Tamura M, Gu Z, Matsushita B and Eklundh L 2004 A simple method for reconstructing a high-quality NDVI time-series data set based on the Savitzky–Golay filter *Remote Sens. Environ.* **91** 332–44
Chen Z, Wang W, Yu Z, Xia J and Schwartz F W 2020 The collapse points of increasing trend of vegetation rain-use efficiency under droughts *Environ. Res. Lett.* **15** 104072
Cowan I R and Farquhar G D 1977 Stomatal function in relation to leaf metabolism and environment *Symp. Soc. Exp. Biol.* **31** 471–505
Dardel C, Kergoat L, Hiernaux P, Grippa M, Mougin E, Ciais P and Nguyen C-C 2014 Rain-use-efficiency: what it tells us about the conflicting sahel greening and Sahelian Paradox *Remote Sens.* **6** 3446–74
Dawson A 2016 eofs: a library for EOF analysis of meteorological, oceanographic, and climate data *J. Open Res. Softw.* **4** e14
de Jong R, de Bruin S, de Wit A, Schaepman M E and Dent D L 2011 Analysis of monotonic greening and browning trends from global NDVI time-series *Remote Sens. Environ.* **115** 692–702
Didan K 2021 MODIS/Terra Vegetation Indices 16-Day L3 Global 250m SIN Grid V061 [Data set] (NASA EOSDIS Land Processes Distributed Active Archive Center) (https://doi.org/10.5067/MODIS/MOD13Q1.061) (Accessed 4 March 2025)
Eyring V, Bony S, Meehl G A, Senior C A, Stevens B, Stouffer R J and Taylor K E 2016 Overview of the coupled model intercomparison project phase 6 (CMIP6)

experimental design and organization *Geosci. Model Dev.* **9** 1937–58
Feng S and Fu Q 2013 Expansion of global drylands under a warming climate *Atmos. Chem. Phys.* **13** 10081–94
Fensholt R *et al* 2012 Greenness in semi-arid areas across the globe 1981–2007—an Earth observing Satellite based analysis of trends and drivers *Remote Sens. Environ.* **121** 144–58
Fensholt R, Rasmussen K, Kaspersen P, Huber S, Horion S and Swinnen E 2013 Assessing land degradation/recovery in the African Sahel from long-term Earth observation based primary productivity and precipitation relationships *Remote Sens.* **5** 664–86
Fick S E and Hijmans R J 2017 WorldClim 2: new 1-km spatial resolution climate surfaces for global land areas *Int. J. Climatol.* **37** 4302–15
Forkuor G, Hounkpatin O K, Welp G, Thiel M and Hui D 2017 High resolution mapping of soil properties using remote sensing variables in South-Western Burkina Faso: a comparison of machine learning and multiple linear regression models *PLoS ONE* **12** e0170478
Friedl M and Sulla-Menashe D 2022 MODIS/Terra+Aqua Land Cover Type Yearly L3 Global 500m SIN Grid V061 [Data set] (NASA EOSDIS Land Processes Distributed Active Archive Center) (https://doi.org/10.5067/MODIS/MCD12Q1.061)
Gonsamo A *et al* 2021 Greening drylands despite warming consistent with carbon dioxide fertilization effect *Glob. Change Biol.* **27** 3336–49
Hänke H, Börjeson L, Hylander K and Enfors-Kautsky E 2016 Drought tolerant species dominate as rainfall and tree cover returns in the West African Sahel *Land Use Policy* **59** 111–20
Haverd V, Smith B, Canadell J G, Cuntz M, Mikaloff-Fletcher S, Farquhar G, Woodgate W, Briggs P R and Trudinger C M 2020 Higher than expected CO_2 fertilization inferred from leaf to global observations *Glob. Change Biol.* **26** 2390–402
He B, Wang S, Guo L and Wu X 2019 Aridity change and its correlation with greening over drylands *Agric. For. Meteorol.* **278** 107663
Holm A M, Cridland S W and Roderick M L 2003 The use of time-integrated NOAA NDVI data and rainfall to assess landscape degradation in the arid shrubland of Western Australia *Remote Sens. Environ.* **85** 145–58
Hussain M M and Mahmud I 2019 pyMannKendall: a python package for non parametric Mann Kendall family of trend tests *J. Open Source Softw.* **4** 1556
Huxman T E *et al* 2004 Convergence across biomes to a common rain-use efficiency *Nature* **429** 651–4
Ji L and Brown J F 2022 Temporal greenness trends in stable natural land cover and relationships with climatic variability across the conterminous United States *Earth Interact.* **26** 66–83
Kaptué A T, Prihodko L and Hanan N P 2015 On regreening and degradation in Sahelian watersheds *Proc. Natl. Acad. Sci. USA* **112** 12133–8
Kim S W, Jung D and Choung Y 2020 Development of a multiple linear regression model for meteorological drought index estimation based on landsat satellite imagery *Water* **12** 3393
Korell L, Auge H, Chase J M, Harpole W S and Knight T M 2021 Responses of plant diversity to precipitation change are strongest at local spatial scales and in drylands *Nat. Commun.* **12** 2489
Körner C, Möhl P and Hiltbrunner E 2023 Four ways to define the growing season *Ecol. Lett.* **26** 1277–92
Le Houérou H N 1984 Rain use efficiency: a unifying concept in arid-land ecology *J. Arid Environ.* **7** 213–47
Lean J L and Rind D H 2008 How natural and anthropogenic influences alter global and regional surface temperatures: 1889–2006 *Geophys. Res. Lett.* **35** L18701
Lehner F, Coats S, Stocker T F, Pendergrass A G, Sanderson B M, Raible C C and Smerdon J E 2017 Projected drought risk in 1.5 °C and 2 °C warmer climates *Geophys. Res. Lett.* **44** 7419–28
Li Z, Wang S, Li C, Ye C, Gao D and Chen P 2022 The trend shift caused by ecological restoration accelerates the vegetation greening of China's drylands since the 1980s *Environ. Res. Lett.* **17** 044062
Lian X *et al* 2021 Multifaceted characteristics of dryland aridity changes in a warming world *Nat. Rev. Earth Environ.* **2** 232–50
Müller L M and Bahn M 2022 Drought legacies and ecosystem responses to subsequent drought *Glob. Change Biol.* **28** 5086–103
Myneni R B and Williams D L 1994 On the relationship between FAPAR and NDVI *Remote Sens. Environ.* **49** 200–11
Nemani R R, Keeling C D, Hashimoto H, Jolly W M, Piper S C, Tucker C J, Myneni R B and Running S W 2003 Climate-driven increases in global terrestrial net primary production from 1982 to 1999 *Science* **300** 1560–3
O'Neill B C *et al* 2016 The scenario model intercomparison project (ScenarioMIP) for CMIP6 *Geosci. Model Dev.* **9** 3461–82
Paruelo J M, Lauenroth W K, Burke I C and Sala O E 1999 Grassland precipitation-use efficiency varies across a resource gradient *Ecosystems* **2** 64–68
Prince S D 2007 Satellite remote sensing of primary production: comparison of results for Sahelian grasslands 1981–1988 *Int. J. Remote Sens.* **12** 1301–11
Rasmussen M S 2010 Developing simple, operational, consistent NDVI-vegetation models by applying environmental and climatic information: part I. Assessment of net primary production *Int. J. Remote Sens.* **19** 97–117
Rifai S W, De Kauwe M G, Ukkola A M, Cernusak L A, Meir P, Medlyn B E and Pitman A J 2022 Thirty-eight years of CO_2 fertilization has outpaced growing aridity to drive greening of Australian woody ecosystems *Biogeosciences* **19** 491–515
Roundy P E 2015 On the Interpretation of EOF analysis of ENSO, atmospheric kelvin waves, and the MJO *J. Clim.* **28** 1148–65
Stern D I and Kaufmann R K 2014 Anthropogenic and natural causes of climate change *Clim. Change* **122** 257–69
Swain D L, Prein A F, Abatzoglou J T, Albano C M, Brunner M, Diffenbaugh N S, Singh D, Skinner C B and Touma D 2025 Hydroclimate volatility on a warming Earth *Nat. Rev. Earth Environ.* **6** 35–50
Thornton M M, Shrestha R, Wei Y, Thornton P E, Kao S-C and Wilson B E 2022 Daymet: Daily Surface Weather Data on a 1-km Grid for North America, Version 4 R1 (ORNL DAAC) (https://doi.org/10.3334/ORNLDAAC/2129)
Thornton P E, Shrestha R, Thornton M, Kao S-C, Wei Y and Wilson B E 2021 Gridded daily weather data for North America with comprehensive uncertainty quantification *Sci. Data* **8** 190
Tippett M K and L'Heureux M L 2020 Low-dimensional representations of Niño 3.4 evolution and the spring persistence barrier *npj Clim. Atmos. Sci.* **3** 1–11
Uddin S, Löw M, Parvin S, Fitzgerald G J, Tausz-Posch S, Armstrong R, O'Leary G and Tausz M 2018 Elevated [CO_2] mitigates the effect of surface drought by stimulating root growth to access sub-soil water *PLoS One* **13** e0198928
Verbruggen W, Schurgers G, Meunier F, Verbeeck H and Horion S 2024 Simulated tree-grass competition in drylands is modulated by CO_2 fertilization *Earth's Future* **12** e2023EF004096
Verón S R, Oesterheld M and Paruelo J M 2005 Production as a function of resource availability: slopes and efficiencies are different *J. Veg. Sci.* **16** 351–4
Volkov D L, Schmid C, Chomiak L, Germineaud C, Dong S and Goes M 2022 Interannual to decadal sea level variability in the subpolar North Atlantic: the role of propagating signals *Ocean Sci.* **18** 1741–62
Wahl E R, Zorita E, Diaz H F and Hoell A 2022 Southwestern United States drought of the 21st century presages drier conditions into the future *Commun. Earth Environ.* **3** 1–14
Wang W, Anderson B T, Entekhabi D, Huang D, Kaufmann R K, Potter C and Myneni R B 2006 Feedbacks of vegetation on summertime climate variability over the North American grasslands. Part II: A Coupled Stochastic Model *Earth Interact.* **10** 1–30

Werb B E and Rudnick D L 2023 Remarkable changes in the dominant modes of North Pacific Sea surface temperature *Geophys. Res. Lett.* **50** e2022GL101078

Wessels K J, Prince S D, Zambatis N, MacFadyen S, Frost P E and Van Zyl D 2006 Relationship between herbaceous biomass and 1-km^2 advanced very high resolution radiometer (AVHRR) NDVI in Kruger National Park, South Africa *Int. J. Remote Sens.* **27** 951–73

Winkler A J *et al* 2021 Slowdown of the greening trend in natural vegetation with further rise in atmospheric CO_2 *Biogeosciences* **18** 4985–5010

Wolf A, Anderegg W R L and Pacala S W 2016 Optimal stomatal behavior with competition for water and risk of hydraulic impairment *Proc. Natl Acad. Sci.* **113** E7222–30

Xue J, Ge Y and Ren H 2017 Spatial upscaling of green aboveground biomass derived from MODIS-based NDVI in arid and semiarid grasslands *Adv. Space Res.* **60** 2001–8

Yue S, Pilon P, Phinney B and Cavadias G 2002 The influence of autocorrelation on the ability to detect trend in hydrological series *Hydrol. Process.* **16** 1807–29

Zhang J, Zhang Y, Cong N, Tian L, Zhao G, Zheng Z, Gao J, Zhu Y and Zhang Y 2023 Coarse spatial resolution remote sensing data with AVHRR and MODIS miss the greening area compared with the Landsat data in Chinese drylands *Front. Plant Sci.* **14** 1129665

Zhang X, Du X and Zhu Z 2020 Effects of precipitation and temperature on precipitation use efficiency of alpine grassland in Northern Tibet, China *Sci. Rep.* **10** 20309

Zhang Y *et al* 2022 Increasing sensitivity of dryland vegetation greenness to precipitation due to rising atmospheric CO_2 *Nat. Commun.* **13** 4875

Zhang Y, Hou J, Han W, Dou P and Huang C 2024 Spatio-temporal analysis of LAI using multisource remote sensing data for source region of Yellow River Basin *Front. Environ. Sci.* **12**

Zhang Y, Wallace J M and Battisti D S 1997 ENSO-like interdecadal variability: 1900–93 *J. Clim.* **10** 1004–20

Zhu X, Liu H, Xu C, Wu L, Shi L and Liu F 2022 Soil coarsening alleviates precipitation constraint on vegetation growth in global drylands *Environ. Res. Lett.* **17** 114008

Zhuang Y, Fu R, Lisonbee J, Sheffield A M, Parker B A and Deheza G 2024 Anthropogenic warming has ushered in an era of temperature-dominated droughts in the western United States *Sci. Adv.* **10** eadn9389